SLAC-PUB-1998
August 1977
(T/E)

RECENT RESULTS ON NEW PARTICLE PRODUCTION AT SPEAR*

R. Schwitters

Stanford Linear Accelerator Center
Stanford University, Stanford, California 94305

Introduction

Over the past three years there have been many talks given on the subject of new particle production and many different particles have been the subjects of these talks. Most of these are rapidly becoming old particles which goes to show just how successful physicists have been in exploring these new phenomena and how insatiable our appetites are for the latest rumors from ever newer discoveries. Therefore, I must be specific in what I mean by new particles; this talk is concerned mainly with the evidence for and properties of the charmed mesons D^o, $D^{\pm}$ and their excited states D^{*o}, $D^{*\pm}$ as measured in the SLAC/LBL magnetic detector at SPEAR. Some very recent results on the structure of R, the ratio of the total cross section for hadron production by e^+e^- annihilation to the point-like muon pair cross section, in the center-of-mass energy $E_{c.m.}$ region near 4 GeV are discussed.

This is not to say that there are no longer problems concerning other aspects of the new physics.[1)] Indeed, there remain important questions concerning details of charmonium spectroscopy, particularly the existence of the pseudoscalar partner of the ψ' and decay modes of the η_c. However, because of the concentration on the 4 GeV region, there is little new information from SPEAR on these questions. Probably the most important single issue in the new particle physics is the existence of a new member of the lepton family. A large body of data, consistent with the hypothesis of a heavy lepton, has been accumulated at SPEAR; this work has been reviewed recently by Perl[2)] and shall not be discussed here. Professor Yamada will discuss some of the recent and important results from DESY on this subject.

---

*Work supported by the Energy Research and Development Administration.

(Invited talk at the 1977 INS International Symposium on New Particles and the Structure of Hadrons, Tokyo, Japan, July 12-14, 1977.)

The SPEAR Program

Currently SPEAR is in a transition period. The SLAC/LBL magnetic detector, which collected all of the data I shall be discussing here, is in the process of being dismantled so that a new device known as the Mark II detector can be installed in the fall of 1977. This new detector will have superior trigger capability, gamma ray detection, solid angle coverage and momentum resolution over the previous one and it should allow us to answer many old new-particle questions as well as learning new things about new particles.

For the past year, a subset of the SLAC half of the SLAC/LBL collaboration, a new LBL group, and physicists from Northwestern University and the University of Hawaii have operated the magnetic detector with a special gamma ray—electron detector known as the "lead glass wall" in order to improve electron and gamma ray detection. This group only now is beginning to present final results and therefore most of the data presented here were accumulated more than a year ago. Also during the past year, physicists from Stanford, UCLA, and the University of California at Irvine began to operate a new detector known as DELCO in SPEAR's second interaction region. This device is well suited for detecting electrons and should provide, in the near future, important new information on leptonic or semileptonic decays of all types of new particles produced at SPEAR energies.

Charmed Particle Production

The success of the charmed quark theory[3)] in explaining the ψ, ψ', and their related χ state spectroscopy and the long list of other highly attractive features of this model were strong impetus to search for charm particle production in e^+e^- annihilation. After our first preliminary search[4)] for charm particle production at SPEAR proved unsuccessful, we accumulated considerably more data in the 4 GeV region and, using improved analysis techniques, we were able to obtain positive evidence for charm particle production just a year ago.[5,6)]

Experimental Details

The data described here were collected by the SLAC/LBL magnetic detector. This device (shown schematically in Fig. 1), its trigger requirements and event

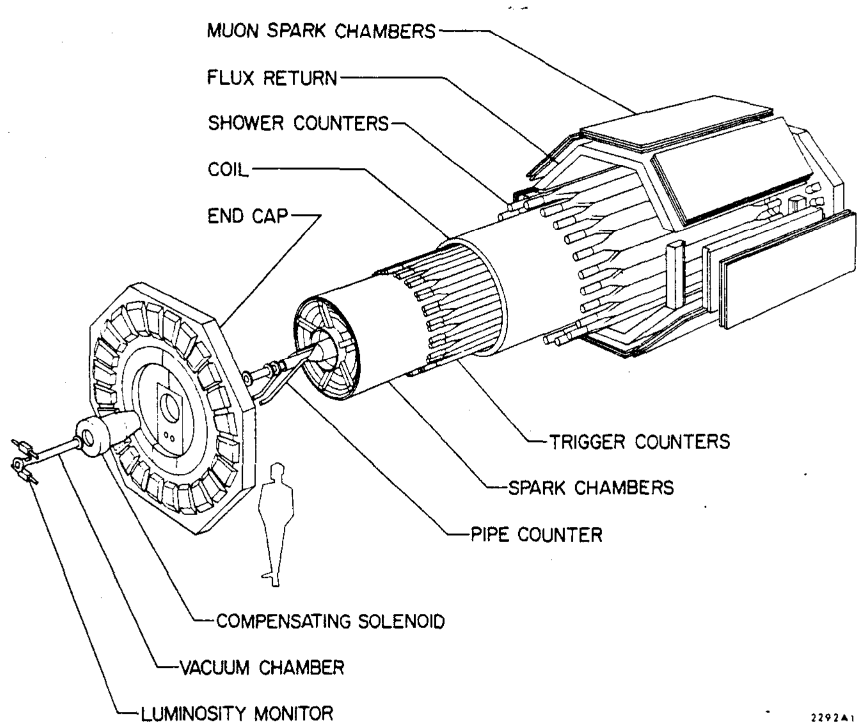

Fig. 1. Exploded view of the SLAC/LBL magnetic detector.

selection procedures have been described previously.[7] The momentum resolution σ_p/p^2 is ± 0.013 $(\mathrm{GeV/c})^{-1}$ for charged particles produced in the beam interaction region, and is worse by about a factor of 1.5 for tracks such as the decay products of K_S^o which cannot be constrained to originate from the beam. The solid angle acceptance for charged tracks is approximately 70% of 4π sr.

An important feature of the detector for charmed particle studies is the time-of-flight (TOF) system which aides in identifying the types of particles observed in hadronic events. The TOF system consists of a cylindrical array of 48 scintillation counters mounted immediately outside of the tracking spark chambers at a radius of 1.5 m from the beam axis. The counters are viewed at both ends by photomultiplier tubes; signals from these phototubes are sent to time-to-digital converters and pulse height converters for making corrections to the TOF information. The beams collide for only about 0.2 nsec every 780 nsec. Thus, an accurate start-time can be associated with every event and the resulting TOF resolution for individual tracks is 0.35 nsec which corresponds to a one standard deviation separation between kaons and pions at 1.3 GeV/c.

Briefly, hadronic events are defined as having three or more charged tracks of momenta greater than about 100 MeV/c which form a vertex within the luminous region of the beams. In some instances, events with only two charged tracks, both of which have momenta greater than 300 MeV/c, where the planes of the two tracks taken with the beam direction are acoplanar by at least 20° and where at least one of the tracks is not an electron are included in the hadron event sample.

The data sample for most of our charm particle studies includes 29,000 hadronic events corresponding to an integrated luminosity of 1830 nb^{-1} recorded over the $E_{c.m.}$ range 3.9 GeV to 4.6 GeV where R was known to exhibit the rich structure shown in Fig. 2. Subsequent to the discovery of a charm particle signal, large samples of data were collected at the fixed values of $E_{c.m.}$, 4.03 GeV and 4.41 GeV where approximately 27,000 and 25,000 hadronic events, corresponding to luminosities of 1270 nb^{-1} and 1630 nb^{-1}, respectively, were recorded.

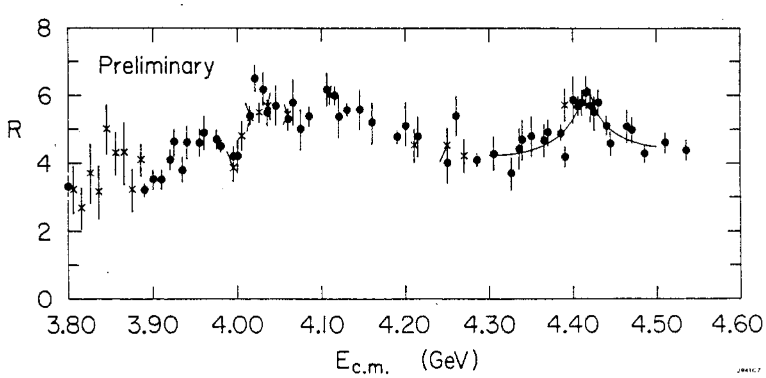

Fig. 2. R, the ratio of the total cross section for hadron production of e^+e^- annihilation to the cross section for muon pair production, in the 4 GeV region of $E_{c.m.}$ where most of the charmed particle studies have been performed.

The time-of-flight information is analyzed in several different ways depending on the particular physics problem being studied. In order to extract maximal information on particle identity, an event-weighting method is used. First, tracks are required to have good timing information consistent with the extrapolated position of the track in the TOF counter. Next, each track is assigned probabilities that it is a π, K, or p; they are determined from the measured momentum and time-of-flight information assuming a Gaussian probability distribution. Tracks with net probability less than 1% are rejected or called pions, depending on the particular kind of analysis being performed. Then, the relative π-K-p probabilities are renormalized so that their sum is unity. Combinations of tracks are weighted by the joint probability that the tracks satisfy the particle-type hypothesis assigned to them. Then, histograms are made by accumulating the event weights. In this way, the total weight assigned to all possible combinations equals the total number of combinations and no double counting occurs.

In much of our analysis, simpler methods can be used. The most common is to assign a set of χ^2 to each track based on the comparison of the time-of-flight recorded for that track and its measured momentum for various hypotheses of particle-type. It is common then to identify kaons as tracks where $\chi^2_K < \chi^2_\pi$, $\chi^2_K < 3$. Other tracks are generally called pions unless they are well identified through TOF as being protons. Generally speaking, there is little difference in these methods when studying combinations of three or more particles in the 4 GeV region. It is only for the case of two-particle combinations where the individual momenta are 1 GeV/c or greater that the weight method sometimes must be used.

The identification of neutral kaons[8)] is based on the measurement of dipion mass and the detection of a vertex, defined by the crossing of the two pion tracks, that is displaced from the beam by at least 10 mm. With the cuts used, the K_s signal to background ratio in the dipion mass interval 480 - 520 MeV/c^2 is typically 2.5. The

K_s^o mass resolution is 18 MeV/c^2 (FWHM) and the measured proper time distribution agrees well with the known K_s^o lifetime.

In most of the analyses discussed here, D-meson candidate events are chosen by invariant mass cuts and backgrounds are estimated from events in adjacent mass bins. In the case of the $K\pi\pi$ decay mode of the D^+, backgrounds are estimated from the nonexotic decay mode $K^{\pm}\pi^+\pi^-$ over the same range of invariant mass as the signal events.

Evidence for D Meson States

Our first direct evidence[5)] of charm particle production by e^+e^- annihilation came from the study of neutral combinations of the charged particles $K\pi$ and $K\pi\pi\pi$. As shown in the top row of Fig. 3, evidence for a new state in the $K\pi$ system appeared in the invariant mass spectrum for all possible neutral combinations of two charged particles assuming both π and K masses for all particles. Through kinematic reflections, the signal appears near 1.74 GeV/c^2 for the $\pi^+\pi^-$ hypothesis, 1.87 GeV/c^2 in the case of $K^+\pi^-$ or $K^-\pi^+$, and 1.98 GeV/c^2 for K^+K^-. To establish the correct choice of final state particles associated with these peaks, the TOF weighting technique was employed. As seen in the second row of Fig. 3, the TOF information dramatically enhances the $K\pi$ signal near 1.87 GeV/c^2. The areas under the small peaks remaining in the $\pi^+\pi^-$ and K^+K^- channels are consistent with the entire signal being $K\pi$ and the resulting misidentification of true $K\pi$ events expected for our TOF system. TOF weighted combinations of the four particles $K\pi\pi\pi$ also showed a significant peak at essentially the same mass. The data of Fig. 3 are consistent with a new state having a mass of 1865 ± 15 MeV/c^2 decaying weakly to the observed particles. The upper limit on the decay width of the state was found to be 40 MeV/c^2.

Studies of recoil mass spectra associated with the new state and searches for its production in very large samples of data at lower values of $E_{c.m.}$ indicated that the threshold energy for producing this new state was above the ψ' mass. The narrow width of this state, its production in association with systems of even greater mass, and the fact that the observed decays involved kaons were strong evidence that this state was the neutral member of the predicted[3)] isodoublet of charmed mesons $(D^o, D^{\mp})$. On the basis of these results, the large blocks of data at $E_{c.m.}$ near 4.03 GeV and 4.41 GeV were accumulated. These data confirmed the D^o signal seen

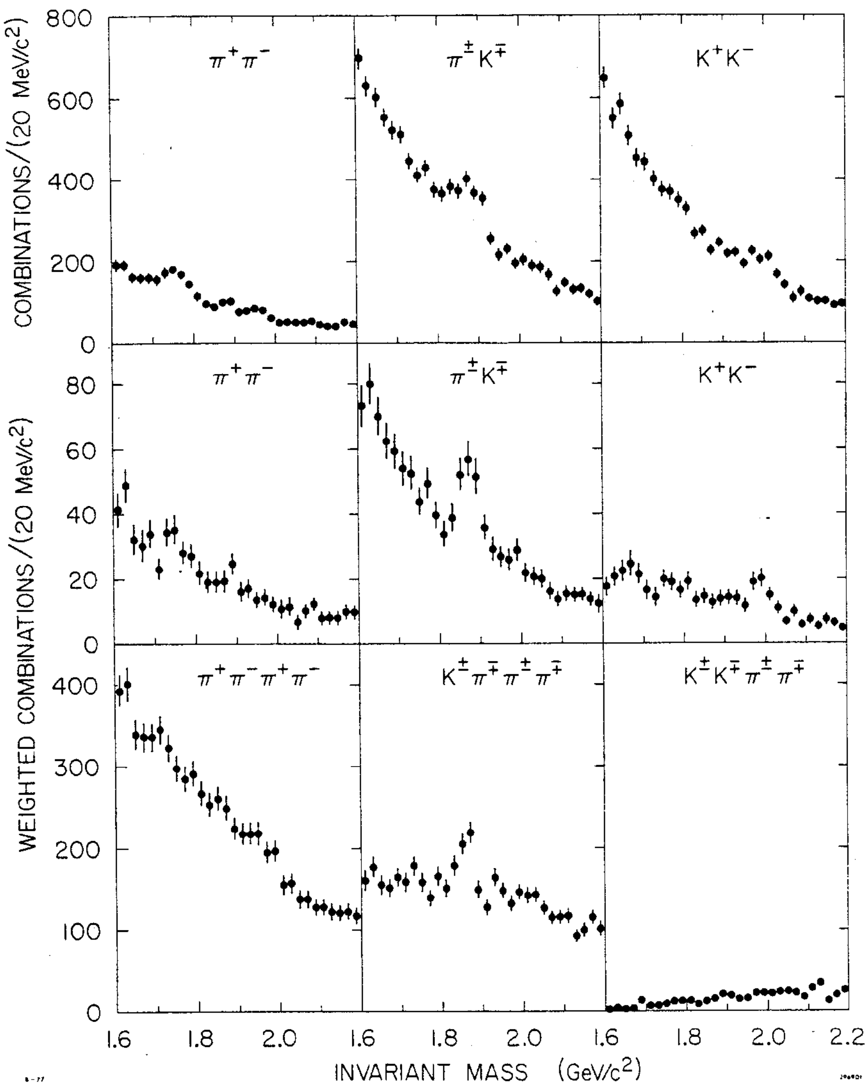

Fig. 3. Invariant mass system for neutral combinations of charged particles. Figures (a), (b), (c) used no TOF information—all possible mass combinations were formed. Figures (d), (e), (f) used the TOF weighting technique and established the K-π decay mode. The four-particle combination in the third row are weighted by TOF probability.

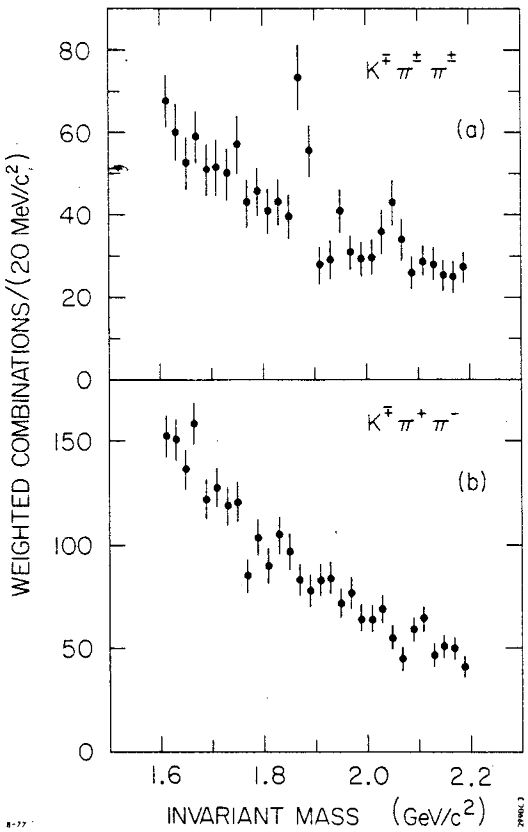

Fig. 4. TOF weighted invariant mass spectra for $K\pi\pi$ combination from 19,000 multihadronic events at $E_{c.m.}=4.028$ GeV. (a) Exotic combinations, $K^{\pm}\pi^{\pm}\pi^{\pm}$, (b) Nonexotic combination $K^{\pm}\pi^{+}\pi^{-}$.

previously and indicated that a narrow charged state at 1876 ± 15 MeV/c^2 which decays into the exotic channel $K^{\pm}\pi^{\mp}\pi^{\mp}$ but not into the normal K* channel $K^{\pm}\pi^{+}\pi^{-}$ was present in e^+e^- annihilation.[9] The evidence for this state is presented in Fig. 4 where TOF weighted invariant mass spectra for exotic and nonexotic combinations of the charged particles $K\pi\pi$ are given. The similarity in mass between this state and the previously reported neutral state, their narrow widths, their recoil mass spectra, their decays to strange particles, and the decay of the charged state to an exotic channel but not to the corresponding normal channel were strong experimental verification of the predictions of Glashow, Iliopoulos, and Maiani.[3]

Recoil mass spectra at the two fixed energies indicated that D's are produced in association with and as decay products of additional excited states D^{*0}, $D^{*\pm}$ having masses near 2.01 GeV/c^2. Figure 5 shows the background-subtracted D^0 recoil mass spectrum at $E_{c.m.}=4.028$ GeV computed assuming a fixed nominal D^0 mass of 1865 MeV/c^2 for both signal and background $K\pi$ combinations. The spectrum is dominated by peaks at 2.01 GeV/c^2 and 2.15 GeV/c^2 with weaker evidence for a peak at 1.87 GeV/c^2 corresponding to $D^0\bar{D}^0$ production. The same spectrum for events collected at $E_{c.m.}=4.414$ GeV is presented in Fig. 5b. The 2.01 GeV/c^2 peak is still

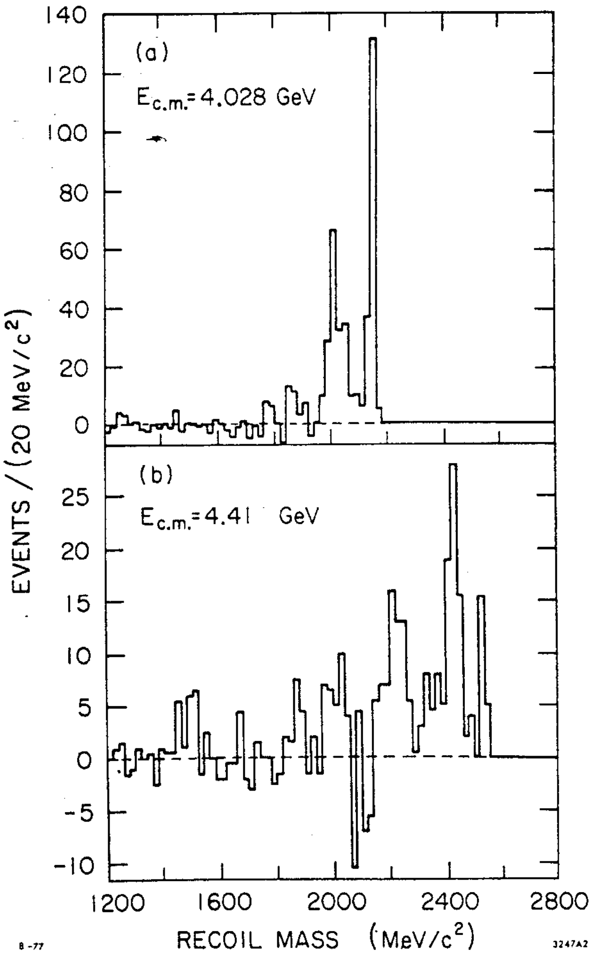

Fig. 5. Recoil mass spectra for D^0 candidates selected from $K\pi$ and $K3\pi$ combinations. (a) $E_{c.m.} = 4.028$ GeV, (b) $E = 4.414$ GeV.

present but the 2.15 GeV/c^2 peak has moved to 2.20 GeV/c^2 and has broadened. From this behavior, we conclude that the 2.01 GeV/c^2 peak represents a state D^{*0} produced in association with the observed D^0 while the other peak moves with $E_{c.m.}$ in the manner expected for a kinematic reflection arising from D^{*0} pair production followed by the decay of D^{*0} to D^0. As discussed below, the detailed shapes of these distributions depend on masses, D^* branching ratios and contributions from the decay $D^{*+} \to \pi^+ D^0$. The data of Fig. 5b also show a peak near the recoil mass 2.43 GeV/c^2 that may represent further excited states of the neutral D system or that could be only kinematic or phase space in origin.

The D^+ recoil mass spectrum at $E_{c.m.} = 4.028$ GeV, shown in Fig. 6, also has a peak near 2.01 GeV/c^2 indicating the existence of the excited state D^{*+}. Direct observation of the D^{*+} became possible[10) through the decay mode $D^{*+} \to D^0\pi^+$. Since the Q value of this decay is small, the momenta of the D^0 and π^+ in the laboratory frame will be roughly proportional to their masses. The efficiency for detecting charged particles with momenta less than 100 MeV/c in the SLAC/LBL magnetic detector is low and, therefore, the D^{*+} decay cannot be readily detected unless the D^0 momentum is 1.5 GeV/c or greater. For this reason some 160,000 hadronic events in the $E_{c.m.}$ range 5.0 GeV to 7.8 GeV

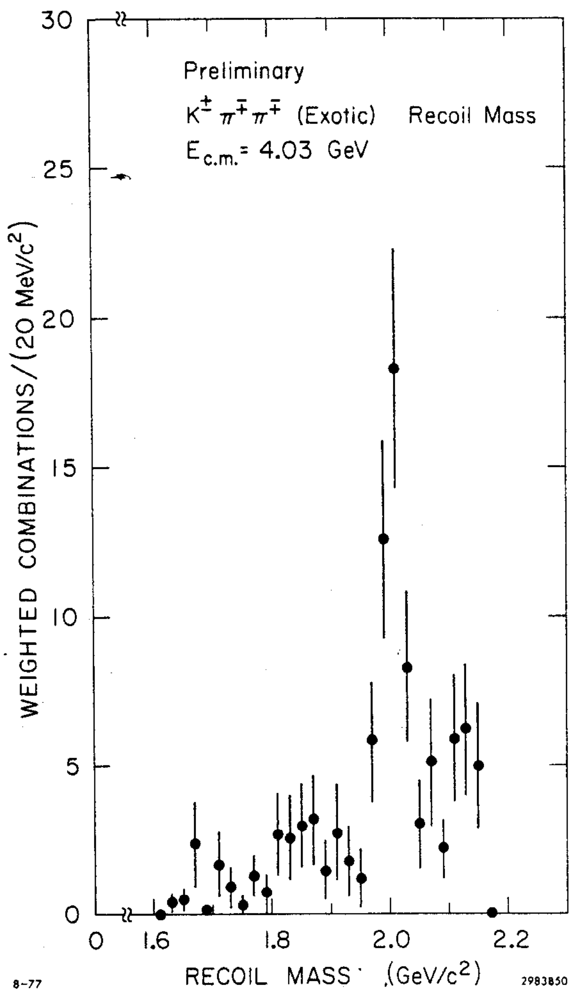

Fig. 6. Recoil mass spectrum for $D^{\pm}$ candidate selected from $K^{\mp}\pi^{\pm}\pi^{\pm}$ combinations at $E_{c.m.}$ = 4.028 GeV.

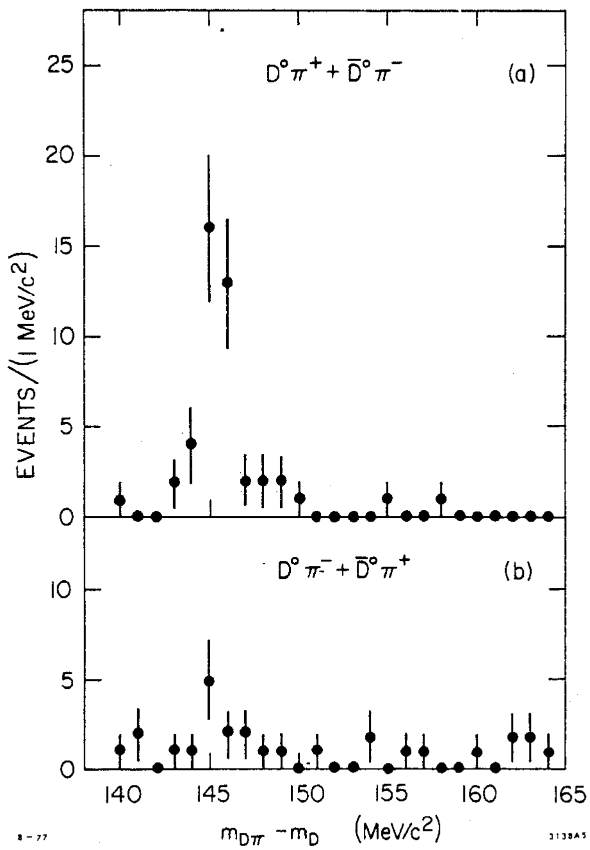

Fig. 7. $D\pi$-D invariant mass difference spectra (a) $D^{0}\pi^{+}$ and $\bar{D}^{0}\pi^{-}$ combination, (b) $\bar{D}^{0}\pi^{+}$ and $D^{0}\pi^{-}$ combinations.

were searched for D^{0} candidates decaying to $K\pi$ with net momentum greater than 1.5 GeV/c. A peak in the $K\pi$ invariant mass spectrum at the D^{0} mass was clearly visible. D^{0} candidates were combined with an additional pion to give the $D\pi$-D mass difference spectrum shown in Fig. 7. In this figure, the designation D^{0} indicates a $K^{-}\pi^{+}$ combination while $\bar{D}^{0}$ is a $K^{+}\pi^{-}$ combination. These data show a strong D^{*+} peak in the channel $D^{0}\pi^{+}$ while there is essentially no signal in the $D^{0}\pi^{-}$ channel. The observed width of the D^{*+} peak in Fig. 7 is consistent with that expected from experimental resolution alone; at the 90% confidence level, the decay width of the D^{*+} is less than 2.0 MeV/c^{2}.

From these data the D^{*+}-D^o mass difference is measured to be 145.3 ± 0.5 MeV/c^2, or equivalently the Q-value of the decay is 5.7 ± 0.5 MeV/c^2. The error is dominated by systematic uncertainties. The implications of these data on questions of D^o-$\bar{D}^o$ mixing are discussed below.

Mass of the D States

In order to measure more precisely the masses of the charged and neutral D and D* states and to study D* decay modes we have examined,[11] in detail, the observed D^o and $D^{\pm}$ momentum spectra at $E_{c.m.}$ = 4.028 GeV and compared them to a model of D and D* production. The $K\pi$ decay mode of D^o and $K\pi\pi$ decay mode of D^+ were selected by χ^2 TOF techniques and invariant mass cuts. Even though a relatively large fraction of $K\pi$ candidates have been assigned the incorrect choice of K-π masses, the resulting error on the measurement of their net momenta is negligible. The spectra are shown in Fig. 8. While the recoil mass spectrum would be equivalent, we chose to fit momentum spectra because momentum is the directly observed quantity and the resolution in this variable (±18 MeV/c) and detection efficiency vary by less than ±10% over the allowed momentum range for both the $K\pi$ and $K\pi\pi$ systems.

The model assumptions are:

a. All D and D* production occurs through the two-body reactions

$$e^+e^- \rightarrow D\bar{D} \quad (1)$$

$$e^+e^- \rightarrow D\bar{D}^* + \bar{D}D^* \quad (2)$$

$$e^+e^- \rightarrow D^*\bar{D}^* \quad (3)$$

b. The allowed D* decay modes are

$$D^{*o} \rightarrow \pi^o D^o \quad (4)$$

$$D^{*o} \rightarrow \gamma D^o \quad (5)$$

$$D^{*+} \rightarrow \pi^o D^+ \quad (6)$$

$$D^{*+} \rightarrow \gamma D^+ \quad (7)$$

$$D^{*+} \rightarrow \pi^+ D^o \quad (8)$$

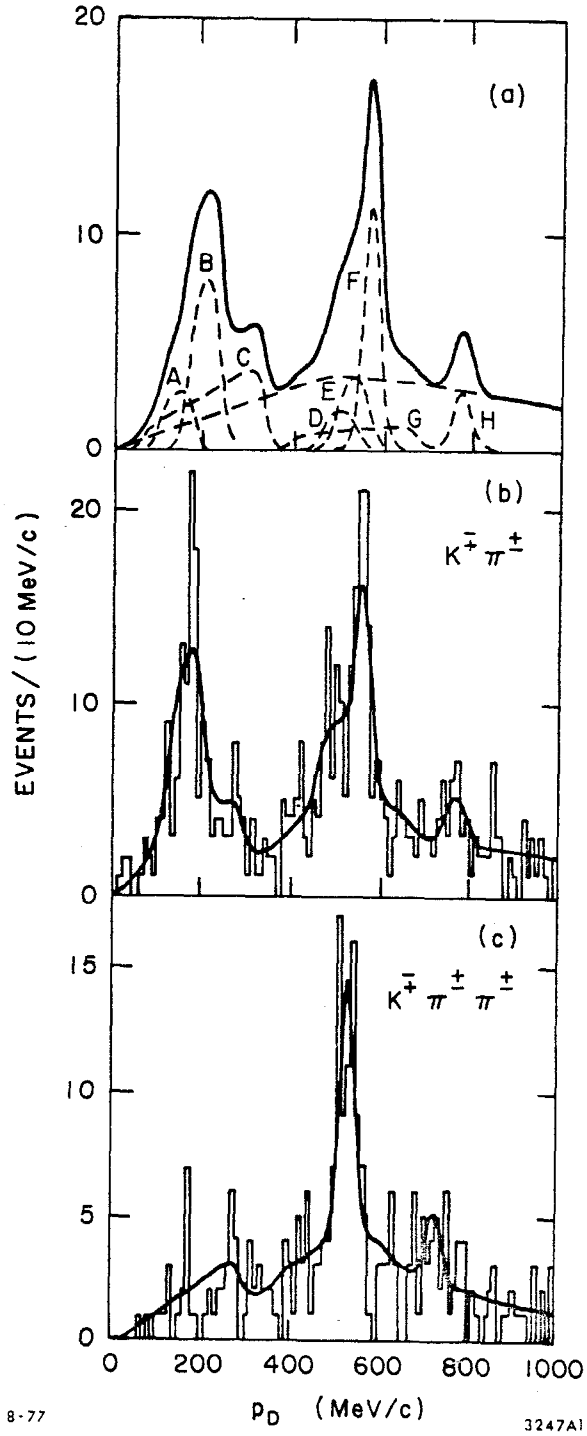

Fig. 8. (a) Illustrative example of the contributions to the expected D^o momentum spectrum near threshold:

$e^+e^- \to D^{*+}D^{*-}$, $D^{*+} \to \pi^+D^o$ (A)

$\to D^{*o}\bar{D}^{*o}$, $D^{*o} \to \pi^oD^o$ (B)

$\to D^{*o}\bar{D}^{*o}$, $D^{*o} \to \gamma D^o$ (C)

$\to D^{*+}D^-$, $D^{*+} \to \pi^+D^o$ (D)

$\to D^{*o}\bar{D}^o$, $D^{*o} \to \pi^oD^o$ (E)

$\to \bar{D}^{*o}D^o$, Direct D^o (F)

$\to D^{*o}\bar{D}^o$, $D^{*o} \to \gamma D^o$ (G)

$\to D^o\bar{D}^o$, Direct D^o (H)

The unlabeled dashed curve corresponds to the smoothed background of uncorrelated $K^-\pi^+$ combinations. (b) $D^o \to K^-\pi^+$ momentum spectrum at $E_{c.m.} = 4.028$ GeV. The solid curve is a typical fit described in text. (c) $D^+ \to K^-\pi^+\pi^+$ momentum spectrum at $E_{c.m.} = 4.028$ GeV compared to a typical fit.

c. D^* decays are isotropic in the D^* rest frame.

Assumption (a) was tested after completing the fits to the spectra discussed below by including in the assumed D^o spectrum a $D^o\bar{D}^o\pi^o$ phase space process. This gave a very broad peak centered near 400 MeV/c that is not seen in the data. We estimate that less than 10% of the D^o signal is from such a process. Reaction (8) complicates the momentum spectra because it couples produced D^{*+} events to observed D^o events. The corresponding $D^{*o} \rightarrow D^+\pi^-$ reaction is kinematically forbidden on the basis of our results. Assumption (c) affects only the shape of momentum spectra for D's produced by reactions (5) and (7) because of their relatively large Q-values. It was found to have a negligible effect on the results by generating Monte Carlo events with the correct angular distributions for the favored D and D^* spins (see below) and fitting the simulated spectra with the simplified model. Fitted parameters agreed well with Monte Carlo input parameters.

D^o and $D^{\pm}$ momentum spectra expected under these assumptions, folded with detector resolution, were fitted simultaneously to the data by varying mass, cross section, and branching ratio parameters. The Q-value for decay mode (8) was fixed at 5.7 MeV through our direct measurement of this process. The momentum spectrum for background events was estimated by smoothing the spectrum observed in candidate background events selected by methods discussed previously. Figure 8a illustrates the contributions to the D^o spectrum from the various processes that were considered in the fits.

The limited statistics, particularly in the D^+ spectrum, preclude the possibility of determining all of the independent parameters describing processes (1) - (8). Therefore, a second fit to the data was performed with the additional assumptions

d. D and D^* are produced at $E_{c.m.} = 4.028$ GeV in states of pure isospin and the phase-space corrections to reactions (1), (2), and (3) follow a p^3 law where p is the center-of-mass momentum.

e. Isospin is a good quantum number in pionic decays of D^* and the transition probability for decay mode (7) is one quarter that of decay mode (5). Phase-space corrections for D^* decay also behave like p^3 where p is now the momentum of the D in the D^* rest frame.

The data were fit under both sets of assumptions with various starting points, background functions, and resolutions in order to study the stability of the results. The solid curves of Figs. 8b and 8c show the results of a typical fit of the second type.

The D^o contribution due to decay mode (8) is highly model dependent. In fits of the first kind, only 6% of the observed D^o's can be attributed to D^{*+} production followed by decay mode (8). In the isospin constrained fits this fraction increases to 29%. Because of this large value, the isospin constrained fit forces the D^{*o} and D^{*+} masses to be nearly equal in order to match the narrowness of the peak near 180 MeV/c in Fig. 8b. It is important to note that the population at low momenta in Fig. 8c is too large to be interpreted as just background. Indeed, if one restricts the $K\pi\pi$ invariant mass analysis to combinations having momenta less than 320 MeV/c, there is a 3 standard deviation peak at the D^+ mass. The natural interpretation of this result is the presence of significant $D^{*+}D^{*-}$ production followed by decays via modes (6) and/or (7).

Decay mode (5) is well established by the data of Fig. 8b. The characteristic triangular momentum spectrum below 300 MeV/c and overall structure between 400 MeV/c and 700 MeV/c demand this reaction. The value for $BR(D^{*o} \to \gamma D^o)$ determined from the isospin constrained fit is a sensitive function of the assumed ratio $s = \frac{\Gamma(D^{*+} \to \gamma D^+)}{\Gamma(D^{*o} \to \gamma D^o)}$. We have assumed s=1/4, but theoretical estimates range from 1/4 to 1/25. As s decreases from 1/4 to 1/16, the fitted value of $BR(D^{*o} \to \gamma D^o)$ increases from 0.75 to 0.90 while no other parameters change appreciably. Values

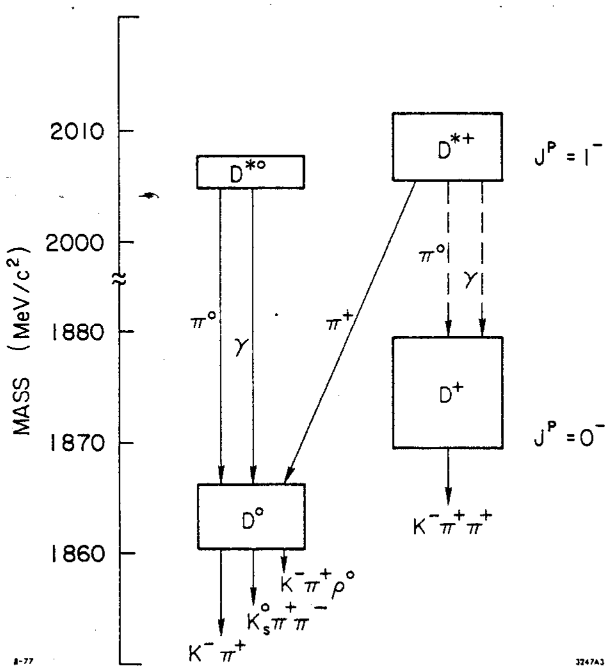

Fig. 9. Summary of masses and observed decay modes for the D meson family. Vertical dimension of boxes indicate one standard deviation error in mass determination. Dashed lines indicate tentative decay modes.

in excess of 0.75, however, no longer fit the triangular portion of the D^0 momentum spectrum below 300 MeV/c. Our final value for this branching ratio including estimated systematic errors is

$$BR(D^{*0} \rightarrow \gamma D^0) = 0.55 \pm 0.15 .$$

The final mass values determined from these fits including estimates of systematic errors are given in the following table.

Table I. Masses of D and D* mesons.

State	Mass (MeV/c)
D^0	1863 ± 3
D^+	1874 ± 5
D^{*0}	2006 ± 1.5
D^{*+}	2008 ± 3

Masses and observed decay modes for the D meson family are summarized in Fig. 9.

Spin Analysis of D^0 and D^{*0}

The analysis described in the previous section indicates that D production near $E_{c.m.} = 4.03$ GeV is dominated by two-body reactions involving D and D* mesons. Considerable information[12)] on the spin and parity of the D^0 and D^{*0} comes from angular distributions of D^0's produced through reactions (2) and (3) and from the observation of decay modes (4) and (5). Both the observation of radiative D^{*0} decay, reaction (5), and $D\bar{D}^*$ production, reaction (2), followed by the π^0 decay mode of D^{*0}, reaction (4), imply that the D^0 and D^{*0} cannot both be spinless. The existence of the pion decay mode of D^{*0}, reaction (4), implies that the D and D* must have even relative parity if one meson has spin 0 and the other has spin 1. Because charmed mesons are associatively produced by strong or electromagnetic interactions, and they decay weakly with parity violations (see below), the absolute parity of the D^0 cannot be determined and thus may be set to -1 by convention. These observations allow unique predictions to be made for the production and decay angular distributions of $K\pi$ combinations arising from the decay of D^0's produced through reaction (2) under the two spin assignments of greatest interest, namely, $J_D = 0$, $J_{D*} = 1$ or the reverse spin assignments.

The expected joint D^0 production and decay angular distribution can be expressed in terms of 3 angles Θ, θ, ϕ where Θ is the polar production angle of the D^0 with respect to the annihilation axis, and (θ, ϕ) are the polar and azimuthal angles of the decay kaon in the D^0 helicity frame. In the limit of nonrelativistic D^{*0} motion, the two possible angular distributions are the following:

$$\frac{d^3\sigma}{d\cos\Theta \, d\cos\theta \, d\phi} \propto 1 + \cos^2\Theta \tag{9}$$

$$\frac{d^3\sigma}{d\cos\Theta \, d\cos\theta \, d\phi} \propto \sin^2\theta \, (\cos^2\phi + \cos^2\Theta \sin^2\phi) \tag{10}$$

Equation (9) is for the case $J_D = 0$, $J_{D*} = 1$ and Eq. (10) is for the case $J_D = 1$, $J_{D*} = 0$.

A relatively clean sample of D^0's produced in association with $\bar{D}^{*0}$ through reaction (2) was obtained by selecting $K\pi$ events on the basis of invariant mass and recoil mass. Using hadron events produced in the $E_{c.m.}$ range 3.9 GeV to 4.15 GeV but predominantly at the fixed $E_{c.m.} = 4.028$ GeV, a sample of 153 D^0 candidates having a recoil mass between 1970 and 2030 MeV/c^2 was obtained. Approximately 15% of this sample is estimated to be background 2-prong combinations. Furthermore, we estimate that $64 \pm 4\%$ of the real D^0's within this cut are primary D^0's recoiling against $\bar{D}^{*0}$. The remaining D^0's come from either pion or gamma decays of the D^{*0} or pion decays of the D^{*+}. The primary fraction exceeds 50% because direct D^0's are partially resolvable from secondary decay D^0's on the basis of the recoil mass cut. The

4% error on this primary fraction is mainly due to uncertainties in the number of D^0's arising from D^{*+} decays.

Figure 10 shows the observed angular distributions for these D^0's candidates. The normalized distributions expected for the two possible spin assignments are also shown. In both figures the solid curve is computed from Eq. (9) and the dashed curve is computed from Eq. (10). The theoretical distributions have been corrected for detector acceptance, resolution, the presence of background events, and the presence of secondary decay D^0's. This last effect is expected to be quite small; we estimate the direction of D^0's arising from π^0 decays of D^{*0} lies within 5^0 of the DD^* axis.

Both possible spin assignments give acceptable fits to the data of Fig. 10a. The third curve shown in Fig. 10a is the $\sin^2 \Theta$ distribution appropriate for the case of spinless D and D*. This spin assignment is clearly ruled out by the data of Fig. 10a with a χ^2 of 74 for 9 degrees of freedom. The main discrimination between the two sets of spin hypotheses

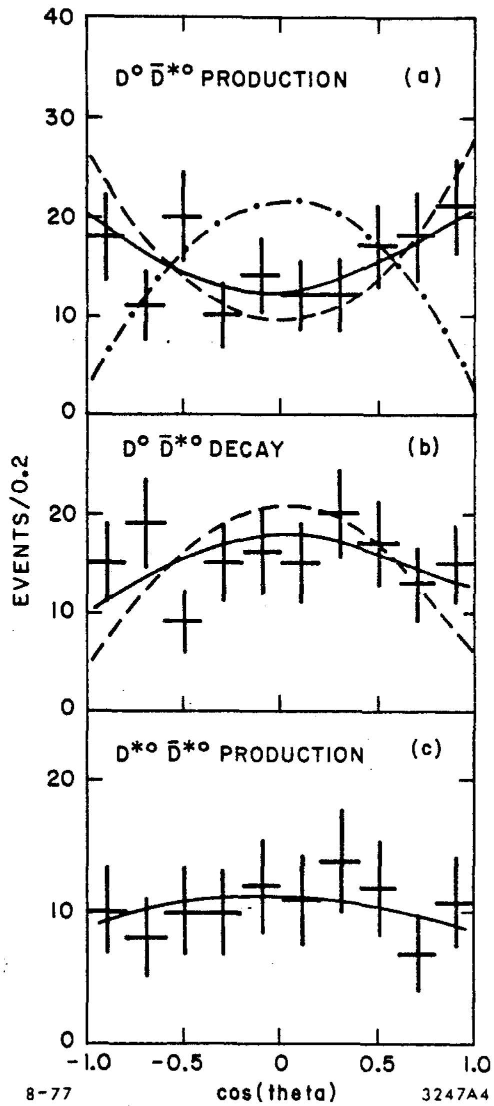

Fig. 10. (a) Production polar distribution of D^0 in reaction (2). Solid curve corresponds to $J^P_D = 0^\pm$ and $J^P_{D*} = 1^\pm$. Dashed curve corresponds to $J_D = 1^\pm$ and $J^P_{D*} = 0^\pm$. Dashed and dotted curve corresponds to spinless D and D*; here "theta" = Θ (see text). (b) Helicity polar distribution for D^0 in reaction (2). Solid curve corresponds to $J^P_D = 0^\pm$ and $J^P_{D*} = 1^\pm$. Dashed curve corresponds to $J^P_D = 1^\pm$ and $J^P_{D*} = 0^\pm$; here "theta" = θ. (c) Production polar distribution for D^0 in reaction (3). Solid curve is deduced from a fit to the form $1 + \alpha \cos^2 \Theta$ where $\alpha = -0.3 \pm 0.3$; here "theta" = Θ.

comes from the kaon polar helicity distribution shown in Fig. 10b. The solid curve is consistent with the data, having a χ^2 of 8.2 for 9 degrees of freedom, while the dashed curve is inconsistent, having a χ^2 of 23 for 9 degrees of freedom ($CL = 6 \times 10^{-3}$). On the basis of this analysis the expected spin assignment, 0 and 1 for D and D*, respectively, is preferred over the alternative assignment.

A second method for discriminating between the two possible spin assignments makes use of all three angular variables simultaneously and handles background differently. The technique is to divide the space of angular variables by a surface of constant $I = \sin^2\theta\,(\cos^2\phi + \cos^2\Theta\,\sin^2\phi)$, such that, the relative populations of events in the two regions offer maximum discrimination between the two spin hypotheses. Figures 11a and 11b show the $K\pi$ invariant mass distributions for events satisfying $I < 0.32$ and $I > 0.32$, respectively. The fits shown in Fig. 11 used a Gaussian signal over an exponentially falling background and give 58 ± 8 events and 73 ± 10 events for the two regions. The difference in a number of signal events divided by their sum is 0.11 ± 0.10 which is in excellent agreement with the value of 0.11 ± 0.01 expected for spin 1 D*'s. The data are inconsistent with the value 0.41 ± 0.03 which is expected for spin 1 D's and spin 0 D*'s. The errors on the expected asymmetries under the two hypotheses

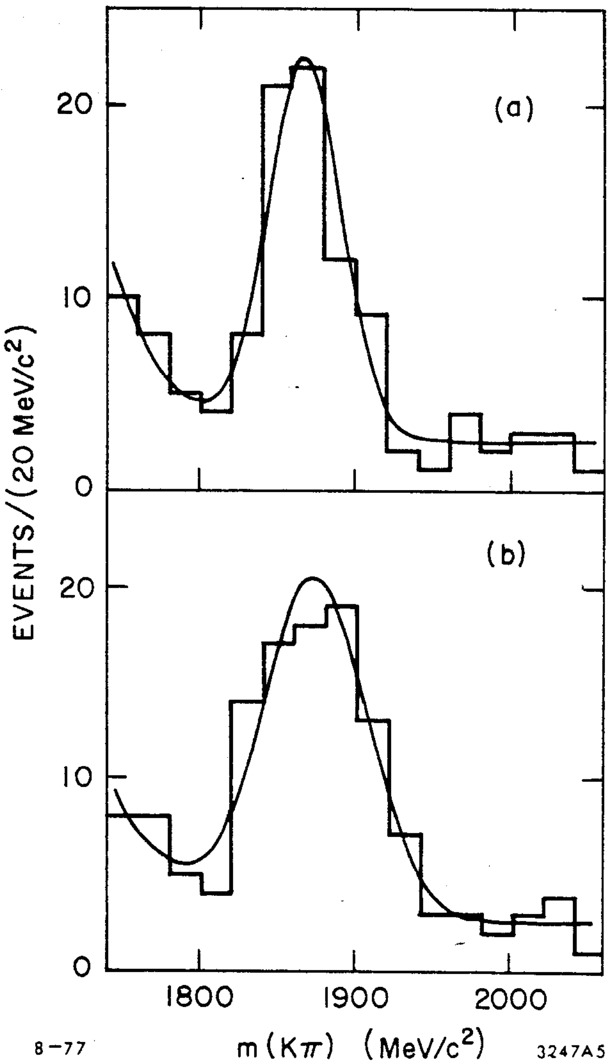

Fig. 11. Invariant mass spectra of $K^{\pm}\pi^{\mp}$ system for $I < 0.32$ and $I > 0.32$.

mainly reflect errors on the fraction of primary D^0's in the data.

Finally, in Fig. 10c the production angular distribution of D^0's from reaction (3) is shown. This reaction can be chosen by selecting D^0's of the appropriate momentum. To a good approximation the observed D^0's follow the initial D^{*0} direction and their measured angular distribution is inconsistent by 2.1 standard deviations from the distribution expected for spinless D^*'s.

In summary, D^0 production near $E_{c.m.} = 4.028$ GeV provides a great deal of information on the spin and parity of D and D* states all of which is consistent with the conventional spin parity assignments 0^-, 1^- for D and D*, respectively. The data rule out the alternative spin assignment 1^-, 0^-, for D and D*.

D^0-$\bar{D}^0$ Mixing

The possibility of significant D^0-$\bar{D}^0$ mixing arising from charm-changing neutral currents has received wide theoretical speculation.[13] We have searched for this effect in two ways. The first method[10] relies on decay mode (8). Since this decay mode conserves the charm quantum number C, the sign of the decay pion is a tag for the value of C for the D^0 system. Thus, if there were no D^0-$\bar{D}^0$ mixing, the sign of the decay pion is correlated with the charge of the kaon arising from the D^0 decay. The data of Fig. 7 clearly demonstrate this correlation. In order to minimize background events from time-of-flight misidentifications, even more restrictive TOF cuts were placed on the data of Fig. 7. Specifically, events within 2.5 MeV/c^2 of the center of the charged D* peak in Fig. 7 were required to have time-of-flight weights for the chosen combination that were three times greater than the weight where the K and π were interchanged. These criteria left 26 events of the expected sign correlation and 3 events of the opposite sign. These 3 events are consistent with coming from backgrounds. It is estimated that 1.4 events arise from uncorrelated combinations of particles and 0.6 events come from $K\pi$ double misidentification. Thus, at the

90% confidence level, the fraction of the time that a D^0 decays as if it were a $\bar{D}^0$ is less than 16%.

The second method for studying D^0-$\bar{D}^0$ mixing[11] is a search for apparent strangeness violation in events containing a D^0 identified through its $K\pi$ decay mode. In the full sample of data taken in the 4 GeV region 77 events were found containing a D^0 candidate and an additional charged kaon. We estimate that 39% of these events correspond to uncorrelated background. In 15 of the events the recoil kaon has the same charge as the D^0 candidate. After background corrections, the fraction of like charges is $12 \pm 9\%$ which is consistent with that expected on the basis of residual TOF misidentification with no D^0-$\bar{D}^0$ mixing. We thus estimate that at the 90% confidence level less than 18% of events containing a D^0 exhibit an apparent strangeness violation.

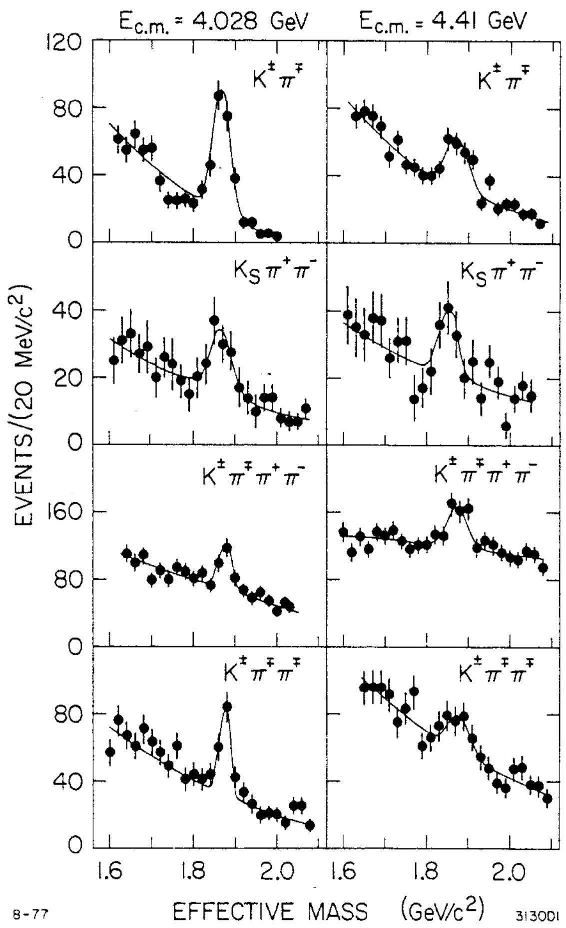

Fig. 12. TOF weighted invariant mass distribution for various particle combinations at $E_{c.m.} = 4.028$ GeV and 4.414 GeV. A recoil mass cut at 1.8 GeV/c^2 has been applied. The curves represent fits to the data.

Production Cross Sections

The weighted mass spectra[14] of $K^\pm\pi^\mp$, $K_s\pi^+\pi^-$, $K^\pm\pi^\mp\pi^\mp$ and $K^\pm\pi^\mp\pi^+\pi^-$ at 4.03 and 4.41 GeV are shown in Fig. 12. To improve the signal to background ratio, only those events for which the recoil mass is larger than 1.8 GeV/c^2 are plotted. All of these channels exhibit significant peaks near 1.87 GeV/c^2 with widths compatible with the experimental resolution. Figure 13 shows the weighted mass spectra of $\pi^+\pi^-$, K^+K^-, $K^\mp\pi^+\pi^-$, $\pi^\mp\pi^+\pi^-$, K^+K^-, $\pi^+\pi^-$, $K_s\pi^\mp$

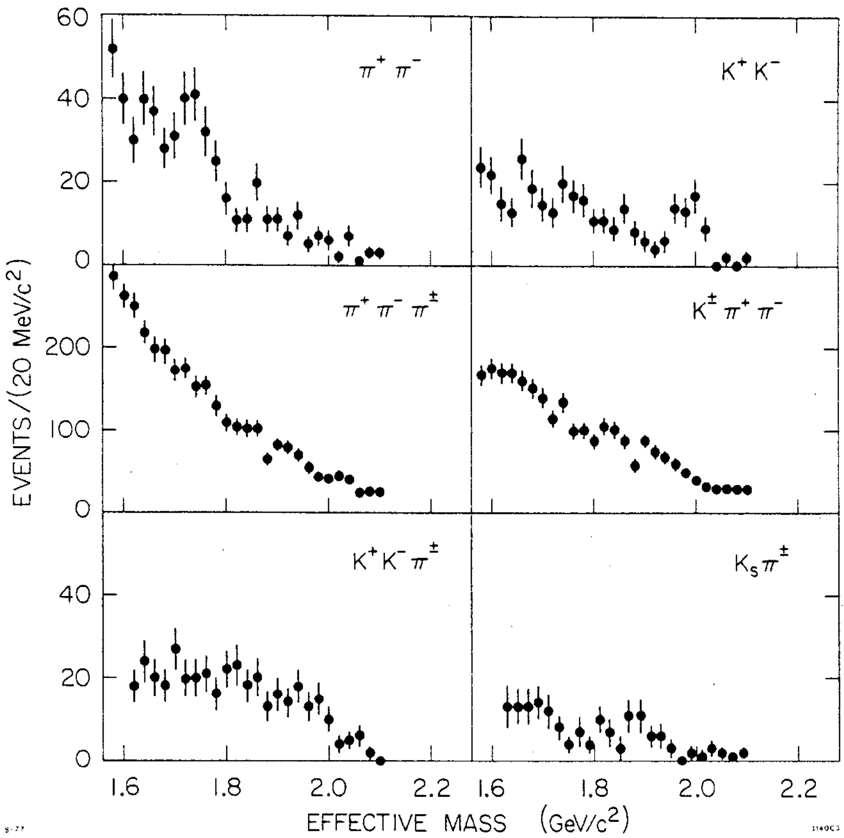

Fig. 13. TOF weighted invariant mass distribution for various particle combinations at $E_{c.m.} = 4.028$ GeV. A 1.8 GeV/c^2 recoil mass cut has been applied.

at 4.03 GeV. The only significant peaks are in the $\pi^+\pi^-$ spectrum at 1.74 GeV/c^2 and in K^+K^- at 1.98 GeV/c^2. These events come from $K\pi$ decays of D^0 in which the K or π have been misidentified. In decay modes with 3 or more particles, this problem does not arise because misidentifications do not yield sharp peaks.

To evaluate D meson populations we have fit each of the mass spectra of Fig. 12 with an adjustable Gaussian superimposed on a polynomial background. The χ^2 per degree of freedom in each case is less than 1. To obtain upper limits for D decay into the channels of Fig. 13, we have to fit each of them with a Gaussian of specified central value and width superimposed on a smooth background.

To go from the weighted event populations to cross sections and branching ratio, a Monte Carlo simulation incorporating all known experimental effects was performed.

In this simulation, production models for D^0 and D^+ which reproduce the observed D momentum spectrum and multiplicities at 4.03 and 4.4 GeV were used.

Table II gives real event populations, efficiencies and values of σB, the product of the D cross section times branching ratio, for the decay modes studied at 4.03 and 4.41 GeV. For those channels in which no significant signal is observed a 90% confidence level upper limit is quoted.

Table II. Event populations, efficiencies and values of σB for several D^0, $\bar{D}^0$ and D^+, D^- decay modes.

Decay Mode	c.m. Energy (GeV)	Number of Events	Detection Efficiency	Cross Section × Branching Ratio σB (nb)
$K^{\mp}\pi^{\pm}$	4.03	182 ± 18	0.25 ± 0.04	0.57 ± 0.11
$\bar{K}^0\pi^+\pi^- + K^0\pi^+\pi^-$		61 ± 14	0.044 ± 0.007	1.09 ± 0.30
$K^{\mp}\pi^{\pm}\pi^+\pi^-$		95 ± 23	0.09 ± 0.02	0.83 ± 0.27
$K^{\mp}\pi^{\pm}\pi^{\pm}$		82 ± 14	0.16 ± 0.03	0.40 ± 0.10
$\bar{K}^0\pi^{\pm} + K^0\pi^{\pm}$		9.5 ± 6.5	0.07 ± 0.01	<0.18
$\pi^-\pi^+$		$5.4^{+8.8}_{-4.5}$	0.27 ± 0.04	<0.04
K^-K^+		$5.2^{+7.5}_{-5.2}$	0.24 ± 0.04	<0.04
$\pi^{\mp}\pi^+\pi^-$		$0.0^{+8.0}_{-0.0}$	0.22 ± 0.03	<0.03
$\pi^{\mp}K^+K^-$		$2.7^{+7.1}_{-2.7}$	0.13 ± 0.03	<0.06
$K^{\mp}\pi^+\pi^-$		$0.0^{+4.7}_{-0.0}$	0.16 ± 0.03	<0.02
$K^{\mp}\pi^{\pm}$	4.41	92 ± 18	0.19 ± 0.04	0.30 ± 0.09
$\bar{K}^0\pi^+\pi^- + K^0\pi^+\pi^-$		55 ± 14	0.037 ± 0.010	0.91 ± 0.34
$K^{\mp}\pi^{\pm}\pi^+\pi^-$		119 ± 41	0.08 ± 0.02	0.91 ± 0.39
$K^{\mp}\pi^{\pm}\pi^{\pm}$		67 ± 19	0.125 ± 0.03	0.33 ± 0.12

The ratio of $D^{\pm}$ production cross sections at 4.41 GeV to 4.03 GeV, determined through its single identified decay mode is about 0.8. The three identified D^{o} decay modes exhibit relative values of σB at 4.41 and 4.03 GeV which do not agree well although the inconsistencies are not outside the level of a reasonable statistical fluctuation. Consequently, we conclude that the ratio of D^{o} cross sections at 4.41 GeV to 4.03 GeV is in the range 0.5 - 1. These ratios do not appear surprising because the hadronic cross section is less at 4.41 GeV than at 4.03 GeV and the cross section for producing new particles other than D mesons may be larger at 4.41 GeV.

If one assigns the total excess cross section of the 4.03 and 4.41 GeV bumps to pair production of charmed mesons, the observed D meson decays amount to roughly 10% of all charmed mesons produced. This low fraction is not surprising because hadronic modes involving neutral mesons other than K^{o} and semileptonic decays cannot be identified in the present detector and decays to higher multiplicity are difficult to detect because of limited solid angle and increasing background.

Decays of the D^{o} to final states of zero strangeness are suppressed relative to states involving a single K meson as can be seen by comparing Figs. 13 and 12. We find that $BR(D^{o} \to \pi^{+}\pi^{-})/BR(D^{o} \to K\pi) < 0.07$ and $BR(D^{o} \to K^{+}K^{-})/BR(D^{o} \to K\pi) < 0.07$ at the 90% confidence level. From weak interaction theory these rates are expected to be suppressed by $\tan^{2}\theta_{c} \sim 0.05$, where θ_{c} is the Cabibbo angle. The same mechanism doubly suppresses the decay of the charged D to nonexotic final states. Our 90% confidence level upper limit for the ratio $BR(D^{\mp} \to K^{\mp}\pi^{+}\pi^{-})/BR(D^{\mp} \to K^{\pm}\pi^{\mp}\pi^{\mp})$ is 0.05.

A byproduct of the detailed fits to the D^{o} momentum spectrum at $E_{c.m.} = 4.028$ GeV is the relative cross sections for the various two-body D^{o} and D^{*o} reactions. Since reactions (1), (2), and (3) are all expected to couple to the virtual photon in a p-wave, a p^{3} phase-space factor is removed from the relative cross sections in order to compare them. The relative importance of reactions (1), (2) and (3) for the D^{o}, D^{*}

channels can therefore be expressed as

$$\begin{array}{ccccc} D^oD^o & & D^oD^{*o} + D^oD^{*o} & : & D^{*o}D^{*o} \\ 0.2 \pm 0.1 & : & 4.0 \pm 0.8 & : & 128 \pm 40 \end{array}$$

These ratios are to be compared with the spin counting estimates[15] of 1:4:7 which are in strong disagreement with the data. Various explanations of this behavior have been discussed in the literature.[15, 16]

Decay Properties of D Mesons

In one of our early studies of D meson properties[17] we observed parity violation in hadronic decays of D mesons. This result follows from the observation that the $K\pi$ decay mode of D^o necessarily forms a state of natural spin-parity $(P = (-1)^J)$. If some other decay mode can be shown to be incompatible with natural spin-parity, then parity violation is established. In our previous study it was explicitly assumed that the D^+ and D^o intrinsic parities were the same. Then the $K\pi\pi$ final state of D^+ was examined for its spin-parity.

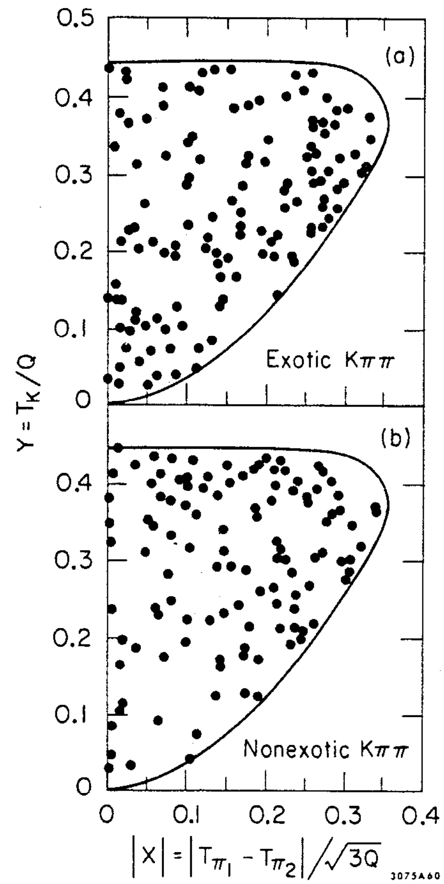

Fig. 14. Dalitz plot (folded around the y-axis) for the $K\pi\pi$ system with the invariant mass cuts, $1.86\ \mathrm{GeV}/c^2 \le M_{K\pi\pi} \le 1.92\ \mathrm{GeV}/c^2$. $Q = T_K + T_{\pi_1} + T_{\pi_2}$, (a) exotic combinations $K^{\mp}\pi^{\pm}\pi^{\pm}$, (b) nonexotic combinations $K^{\pm}\pi^{+}\pi^{-}$.

The Dalitz plot for $K^{\pm}\pi^{\mp}\pi^{\mp}$ events in the D^+ mass range is presented in Fig. 14a. There are 126 events in this Dalitz plot of which it is estimated that 58 are background. In Fig. 14b, a background Dalitz plot is presented consisting of 112 nonexotic $K\pi\pi$ combinations satisfying the same mass and recoil mass cuts. Both signal and background are consistent with uniform population density. A uniformly populated Dalitz plot is incompatible with a $K\pi\pi$ final state of pure natural spin-parity; in the case of a natural spin-parity state decaying into three pseudoscalers, one expects a depopulation along the boundary.[18]

Since three pseudoscalars cannot be in a 0^+ spin-parity state, 1^- and 2^+ exhaust natural spin parity combinations for spin less than 3. In order to make quantitative comparisons, sample matrix elements for these two natural spin-parity states were constructed. The Dalitz plot was then divided into two regions separated by contours of constant density according to the assumed matrix element. The boundary was chosen to give equal population for phase-space decay. These Dalitz boundaries are indicated in Fig. 15 along with the invariant mass spectra of $K\pi\pi$ combinations within the indicated regions. In both cases the data nearly equally populate the two regions of the Dalitz plot whereas the expected distributions for natural spin-parity strongly favor the central region. These results are summarized in the following table.

Table III. Summary of Dalitz plot analysis of $K^{\mp}\pi^{\pm}\pi^{\pm}$ system for three choices of spin-parity assignments.

Spin-Parity Hypothesis	Dalitz Plot Ratios (center/periphery)	Observed Event Ratios (center/periphery)	χ^2/1 DF
1^-	8.2:1	38 ± 9/34 ± 8	18.1
0^-	1:1		0.1
2^+	5.6:1	35 ± 10/31 ± 9	9.4
0^-	1:1		0.1

Thus, the distribution in the Dalitz plot is incompatible with the zeros expected for spin and parity 1^- or 2^+ for the $K\pi\pi$ state and parity nonconservation follows.

The uniform Dalitz plot density shown in Fig. 14 rules out a significant $K^*(890)\pi$ component to charged D decays. Similarly it is found[14] that within the limited statistics, the $D^0 \rightarrow K_S\pi^+\pi^-$ decay mode does not exhibit either K^* or ρ signals at a

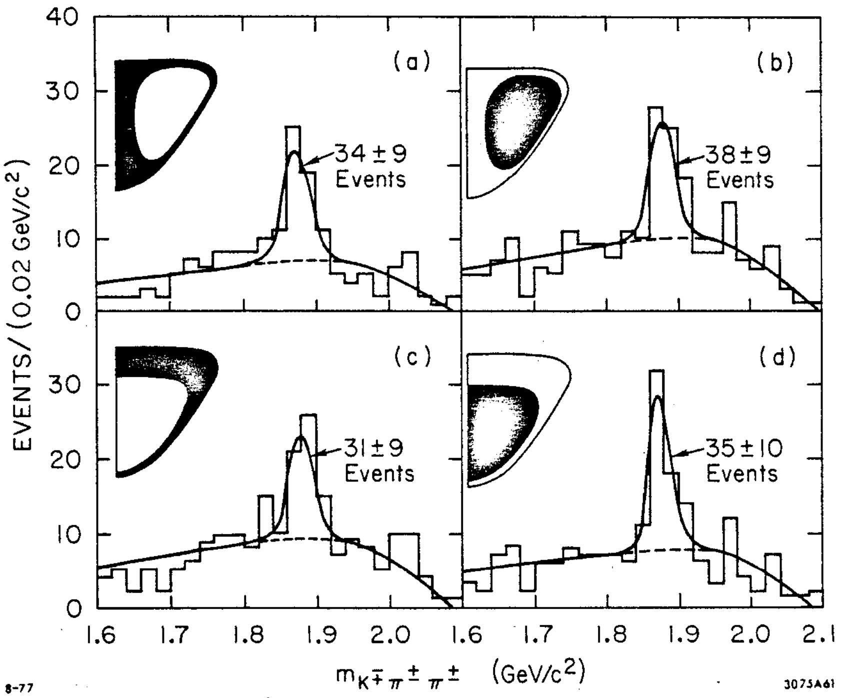

Fig. 15. $K\pi\pi$ invariant mass spectra for events selected from different regions of the $K\pi\pi$ Dalitz plot (a) "peripheral" and (b) "central" regions for a contour of constant intensity for a 1^- matrix element as indicated by the shaded regions of the inserts, (c) "peripheral" and (d) "central" regions for a contour of a 2^+ matrix element. The solid curves are fits to a Gaussian signal to extract numbers of events.

substantial level. However, we find that the $D^o \to K^{\pm}\pi^{\mp}\pi^{+}\pi^{-}$ decay is dominated by the intermediate state $K^{\pm}\pi^{\mp}\rho^o$.

Figure 16a shows the invariant mass for $K3\pi$ combinations having at least one of the two neutral dipions within a ρ^o cut defined from 650 to 850 MeV/c^2. Figure 16b shows the invariant mass for $K3\pi$ combinations which have no neutral dipions within the ρ^o cut. We estimate that 85 ± 15% of the total $K3\pi$ signal resides in Fig. 16a. This ρ^o fraction is substantially larger than the 47% predicted by $K3\pi$ phase-space but consistent with the 81% predicted by a pure $K\pi\rho^o$ final state.

To search for the presence of $K^*(890)$ we define a K^{*o} mass region from 820 to 960 MeV/c^2. We evaluate the fraction of events in $K3\pi$ signal which have at least one of the two $K\pi$ combinations in this K^{*o} region and also the fraction of events which have both a $K\pi$ in the K^{*0} band and the remaining $\pi\pi$ in the ρ region.

Assuming that the $K3\pi$ signal is the sum of the four decays, direct $K3\pi$, $K^{*0}\pi^+\pi^-$, $K\ \pi^{\mp}\rho^0$, $K^{*0}\rho^0$, we unfold the signal fractions by comparison with Monte Carlo calculations for each mode. The results of the fit are summarized below.

Table IV. Summary of the fractions of resonance and nonresonance production in $K3\pi$ decays of D^0.

Phase-Space	$K^{\pm}\pi^{\mp}\rho^0$	$K^*\pi^+\pi^-$	$K^*\rho^0$
$0.05^{+0.1}_{-0.05}$	$0.85^{+0.11}_{-0.22}$	$0.00^{+0.2}_{-0.0}$	$0.10^{+0.11}_{-0.10}$

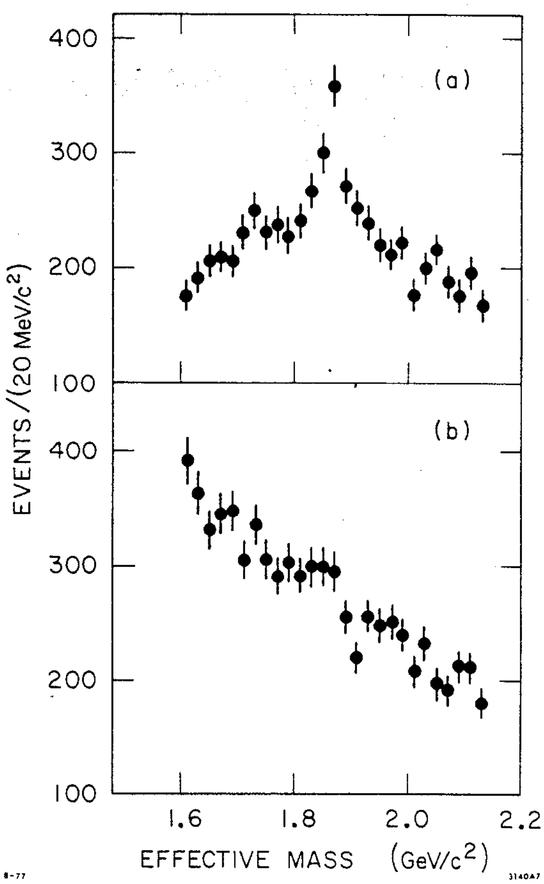

Fig. 16. Evidence for $K\pi\rho$ decay mode of D^0. $K^{\mp}\pi^{\pm}\pi^+\pi^-$ invariant mass spectra for (a) combination with at least one $\pi^+\pi^-$ pair in the ρ^0 mass region 650-850 MeV/c^2, (b) combinations where no $\pi^+\pi^-$ pair is in the ρ^0 mass region.

Remarkably enough, there is no significant K* production whereas $K^{\pm}\pi^{\mp}\rho^0$ seems to be the dominant mode. We find no evidence of A_2 and set a 90% confidence level upper limit of 0.06 for the ratio of $K^{\pm}A_2^{\mp}$ to total $K3\pi$ rates. Theoretical expectations for resonance production in D decay have been discussed in the literature.[19)]

Summary

In summary, the first year of experimental charmed meson physics has yielded important information on the masses, spins and other properties of charged and neutral D and D* mesons. This general body of data is in excellent agreement with the theoretical expectations of the charmed quark theory.

Observation of Another New Resonance at SPEAR

The group of physicists from SLAC/LBL, Northwestern University and the University of Hawaii that added the lead glass wall to the SLAC/LBL magnetic detector has recently observed[20] a resonance in the total cross section for producing hadrons by e^+e^- annihilation in the shadow of the ψ'. The experimental methods and analysis techniques used to determine R in this energy range are essentially identical to those used previously by the SLAC/LBL group.[21]

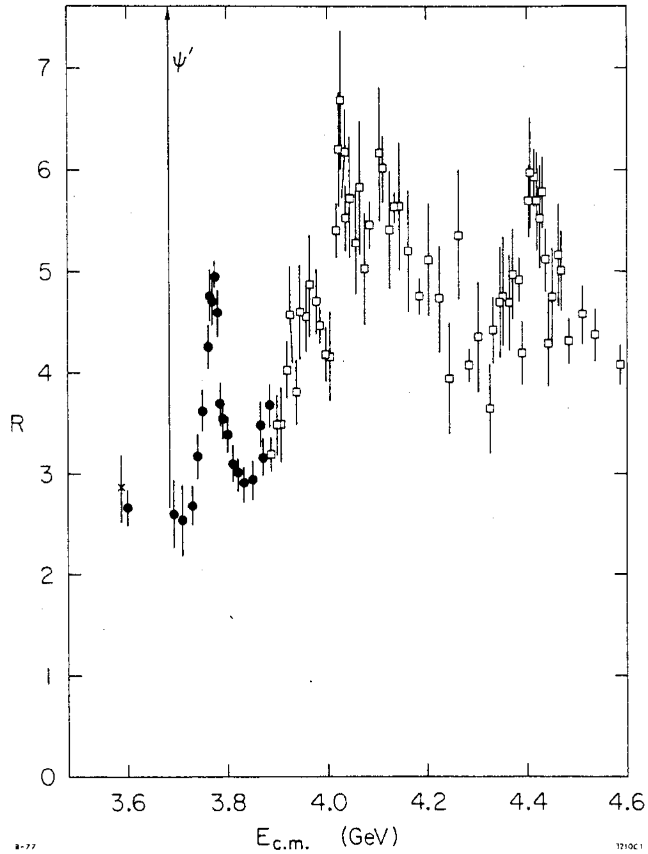

Fig. 17. R vs. $E_{c.m.}$ in the region above the ψ'. Solid points are from the new measurement of Rapidis et al.[20] Other points are from the older SLAC/LBL measurements.[21]

Their values for R the ratio of the total hadronic cross section to the point-like muon pair cross section at energies just above the ψ' mass are presented in Fig. 17. A clear resonance at a mass of 3772 ± 6 MeV/c^2 having a total width of 28 ± 5 MeV/c^2 is evident. The data of Fig. 17 have been corrected for radiative effects arising from the continuum, the tail of the ψ, the tail of the ψ', and the resonance at 3.77 GeV itself. The parameters of this resonance are compared with the other isolated ψ resonances in Table V.

The parameters of the $\psi(3772)$ are in excellent agreement with those predicted by Eichten et al.[22] for the $^3D_1$ state of charmonium. In a nonrelativistic approximation a D-state does not couple to e^+e^-. It can obtain a leptonic width, however, by mixing an S-state. It is normally assumed that the $^3D_1$ mixes primarily with the ψ'. In this approximation one can calculate from the data in Table V that the mixing angle is 23 ± 3^{o}.

Table V. Summary of resonance parameters for the isolated ψ resonances.

State	Mass (MeV/c^2)	Γ (MeV/c^2)	Γ_{ee} (keV/c^2)	B_{ee}
ψ(3095)	3095 ± 4	0.069 ± 0.015	4.8 ± 0.6	0.069 ± 0.009
ψ(3684)	3684 ± 5	0.228 ± 0.056	2.1 ± 0.3	$(9.3 \pm 1.6) \times 10^{-3}$
ψ(3772)	3772 ± 6	28 ± 5	0.37 ± 0.09	$(1.3 \pm 0.2) \times 10^{-5}$
ψ(4414)	4414 ± 7	33 ± 10	0.44 ± 0.14	$(1.3 \pm 0.3) \times 10^{-5}$

This resonance is immediately above $D\bar{D}$ threshold yet preliminary indications are that D meson production is copious. As in the case of the peak at 4.028 GeV, the ψ(3772) should provide important information on the properties of D^{o}, $D^{\pm}$ without the complications due to D* decays.

Acknowledgements

With the exception of the final topic reported here, all of the experimental results discussed above were the work of the SLAC/LBL collaboration working at SPEAR. Physicists who participated in this work are G. S. Abrams, M. S. Alam, A. M. Boyarski, M. Breidenbach, W. C. Carithers, W. Chinowsky, S. Cooper, J. M. Dorfan, G. J. Feldman, G. Goldhaber, G. Hanson, J. A. Jaros, A. D. Johnson, J. A. Kadyk, R. R. Larsen, D. Lüke, V. Lüth, H. L. Lynch, R. J. Madaras, C. C. Morehouse, H. K. Nguyen, J. M. Paterson, M. L. Perl, I. Peruzzi, M. Piccolo, F. M. Pierre, T. P. Pun, P. Rapidis, B. Richter, R. H. Schindler, J. Siegrist, W. Tanenbaum, G. H. Trilling, and J. E. Wiss.

The author also wishes to express his gratitude to the organizing committee of the INS International Symposium and to the other Japanese colleagues for making his first visit to Japan such a pleasant one.

References

1) G. J. Feldman and M. L. Perl, Stanford Linear Accelerator Center preprint SLAC-PUB-1972 (1977), submitted to Physics Reports. Frederick J. Gilman, Proc. of the Ann. Meeting of the American Physics Society DPF, Brookhaven, October 6-8, 1976, report BNL 50598 (1977), p. B19. B. H. Wiik, Proc. of the XVIII Int. Conf. on High Energy Physics, Tbilisi, 1976.

2) M. L. Perl, Stanford Linear Accelerator Center preprint SLAC-PUB-1923, to be published in the Proc. of the XII Rencontre de Moriond, edited by Tran Thanh Van, R.M.I.E.M. Orsay (1977).

3) J. D. Bjorken and S. L. Glashow, Phys. Rev. Letters 11, 255 (1964). S. L. Glashow, J. Iliopoulos, and L. Maiani, Phys. Rev. D 2, 1285 (1970). M. K. Gaillard, B. W. Lee, and J. L. Rosner, Rev. Mod. Phys. 47, 277 (1975).

4) A. M. Boyarski et al., Phys. Rev. Letters 35, 196 (1975).

5) G. Goldhaber et al., Phys. Rev. Letters 37, 255 (1976).

6) Other indications of charmed particle production had come from neutrino experiments, e.g., A. Benvenuti et al., Phys. Rev. Letters 34, 419 (1975); E. G. Cazzoli et al., Phys. Rev. Letters 34, 1125 (1975); J. Bleitschau et al., Phys. Letters 60B, 207 (1976); J. von Krogh et al., Phys. Rev. Letters 36, 710 (1976); B. C. Barish et al., Phys. Rev. Letters 36, 939 (1976).

7) J.-E. Augustin et al., Phys. Rev. Letters 34, 233 (1975); J.-E. Augustin et al., Phys. Rev. Letters 34, 764 (1975).

8) V. Lüth et al., Stanford Linear Accelerator Center preprint SLAC-PUB-1947 (1977), to be published in Phys. Letters.

9) I. Peruzzi et al., Phys. Rev. Letters 37, 569 (1976).

10) G. J. Feldman et al., Phys. Rev. Letters 38, 1313 (1977).

11) G. Goldhaber et al., Stanford Linear Accelerator Center preprint SLAC-PUB-1973 (1977), to be published in Phys. Letters.

12) H. K. Nguyen et al., Phys. Rev. Letters 39, 262 (1977).

13) See, for example, S. L. Glashow and S. Weinberg, Phys. Rev. D 15, 1958 (1977); E. A. Paschos, Phys. Rev. D 15, 1966 (1977); and references to earlier work quoted therein.

14) M. Piccolo et al., Stanford Linear Accelerator Center preprint SLAC-PUB-1978 (1977), submitted to Phys. Letters.

15) A. De Rújula, H. Georgi, and S. L. Glashow, Phys. Rev. Letters 37, 398 (1976); K. Lane and E. Eichten, Phys. Rev. Letters 37, 477 (1976).

16) Y. Iwasaki, Prog. Theor. Phys. 54, 492 (1975); M. Bander et al., Phys. Rev. Letters 36, 695 (1976); C. Rosenzweig, Phys. Rev. Letters 36, 697 (1976); L. B. Okun and M. B. Voloshin, JETP Letters 23, 333 (1976); S. Nussinov and D. P. Sidhu, Fermilab report FERMILAB-Pub-76/70-THY (1976); A. De Rújula, H. Georgi, and S. L. Glashow, Phys. Rev. Letters 38, 317 (1977).

17) J. E. Wiss et al., Phys. Rev. Letters 37, 1531 (1976).

18) C. Zemach, Phys. Rev. B133, 1201 (1964); B. W. Lee, C. Quigg, and J. L. Rosner, Fermilab report FERMILAB-Pub-76/73-THY (1976), unpublished.

19) S. R. Borchardt, T. Goto, and V. S. Mathur, Phys. Rev. D 15, 2022 (1977).

20) P. A. Rapidis et al., Stanford Linear Accelerator Center preprint SLAC-PUB-1959 (1977), submitted to Phys. Rev. Letters (1977).

21) J. Siegrist et al., Phys. Rev. Letters 36, 700 (1976).

22) E. Eichten et al., Phys. Rev. Letters 34, 369 (1975); Phys. Rev. Letters 36, 500 (1976). Also see Lane and Eichten, Ref. 15.